

Structural Transition in the Hidden Ordered Phase of CeCoSi

Takeshi Matsumura¹, Suguru Kishida¹, Mitsuru Tsukagoshi¹, Yukihiro Kawamura², Hironori Nakao³, and Hiroshi Tanida⁴

¹Department of Quantum Matter, ADSE, Hiroshima University, Higashi-Hiroshima, Hiroshima 739-8530, Japan

²Muroran Institute of Technology, Muroran, Hokkaido 050-8585, Japan

³Photon Factory, Institute of Materials Structure Science, High Energy Accelerator Research Organization, Tsukuba, Ibaraki, 305-0801, Japan

⁴Liberal Arts and Sciences, Toyama Prefectural University, Imizu, Toyama 939-0398, Japan

We have performed X-ray diffraction experiments on a single crystalline CeCoSi to investigate the unresolved ordered phase below $T_0 \sim 12$ K. We have discovered that a triclinic lattice distortion takes place below T_0 , which is further modified in the subsequent antiferromagnetic ordered phase. The structural domains can be selected by applying a magnetic field, indicating that some electronic ordering exists behind and affects the magnetic anisotropy in the hidden ordered phase below T_0 . The transition at T_0 , although the order parameter is still unknown, is associated with the maximum in the c -axis lattice parameter. In magnetic fields along $[100]$, the structural transition temperature, named as T_{s1} , deviates from T_0 and decreases with increasing the field, whereas T_0 increases. This shows that the hidden ordered phase without triclinic distortion exists between T_{s1} and T_0 . The results for $H \parallel [110]$ are also reported.

(March 9, 2022)

arXiv:2203.03879v1 [cond-mat.str-el] 8 Mar 2022

1. Introduction

Inter-ionic interactions between localized f -electron orbitals through hybridization with the conduction electrons give rise to a rich variety of ordered phases of multipole moments.¹⁾ In most cases, the order parameters are described by even-parity multipole moments, such as magnetic dipole, electric quadrupole, and magnetic octupole moments, which are inherently allowed in centrosymmetric environments. When the spatial inversion symmetry is locally broken at the magnetic ion site, hybridization with the on-site d orbital is allowed, leading to an occurrence of local odd-parity multipoles.²⁾ Even when a crystal has an inversion center, ferroic order of a cluster-type odd-parity multipole can sometimes be constructed from a staggered ordering of even-parity multipoles, which has been attracting interest as a key concept to understand distinctive magnetoelectric phenomena and unusual ordered phases.³⁾

CeCoSi, with a tetragonal CeFeSi-type structure (space group $P4/nmm$, No. 129), undergoes an antiferromagnetic (AFM) order at $T_N = 9.4$ K.⁴⁻⁸⁾ The crystal structure, drawn by using the program VESTA,⁹⁾ is shown in Fig. 1. The magnetic order is described by a propagation vector $\mathbf{q} = (0, 0, 0)$, where the two Ce atoms in the unit cell, located at noncentrosymmetric sites, are antiferromagnetically coupled.¹⁰⁾ This ordering breaks the global inversion symmetry of the crystal, and gives rise to a cluster-type odd-parity multipole. The crystalline electric field (CEF) level scheme has been determined by inelastic neutron scattering; the ground state is the $\Gamma_7^{(1)}$ doublet and the $\Gamma_7^{(2)}$ and the Γ_6 excited doublets are located at 10.49 meV and at 14.1 meV, respectively.¹⁰⁾ The ground-state wave function is close to that of the Γ_7 doublet in cubic CEF, resulting in an almost isotropic character. The proposed wave functions well explain the nearly isotropic magnetic properties of CeCoSi. It is remarked, however, the size of the ordered moment is less than the value expected from the ground state and is reduced to $0.37 \mu_B$.¹⁰⁾

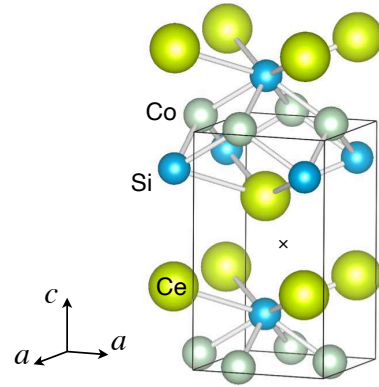


Fig. 1. (Color online) Crystal structure of CeCoSi. $a = 4.057$ Å and $c = 6.987$ Å at room temperature.⁷⁾ A unit cell, represented by the rectangular parallelepiped, contains two formula units. The cross at the midpoint of the two Ce atoms in the unit cell represents the inversion center of the crystal. The Ce atoms are at the $2c$ site $(1/4, 1/4, z)$ ($z = 0.678$) with the site symmetry $4mm$.

Another noteworthy feature in CeCoSi is the unresolved transition at $T_0 \sim 12$ K. Although it has been only detectable as a small anomaly in magnetic susceptibility and specific heat, it is now established to exist as an intrinsic transition by microscopic NQR and NMR measurements.¹¹⁾ In addition, the transition at T_0 is enhanced by applying a high pressure and is connected to the clear anomaly above ~ 1.5 GPa with a gap formation in the conduction band. Therefore, the ordering at T_0 is named as a pressure induced ordered phase (PIOP). The transition temperature reaches to an extremely high value of ~ 36 K at 1.5 GPa, suggesting an unusual c - f hybridization effect.⁵⁻⁷⁾ The NQR and NMR study concludes that the transition is nonmagnetic in nature.¹¹⁾

It is also important that T_0 increases by applying a magnetic field, suggesting a mixing-type quadrupole order by incorporating the excited state. It is for the moment a possible

candidate for the ordered phase in question as discussed in CeTe, or in an extreme case for YbSb.^{12–16} However, in a straightforward consideration, such a scenario is difficult to accept because the energy level of the excited state in CeCoSi is too high to have any effect on the phase transition. This is the mystery of the hidden order at T_0 . Although it has been discussed in association with the cluster-type odd-parity multipole,^{17,18} it is still unclear whether the lack of local inversion symmetry at the Ce site, or the formation of cluster-type odd-parity multipole, play any role in this ordering, which is one of the main issues in CeCoSi.

To study the mysterious ordered phase of CeCoSi between T_N and T_0 from structural viewpoints, we have performed X-ray diffraction experiments. The crystal structure has been considered to maintain the tetragonal symmetry in the whole temperature range as concluded from the results of neutron powder diffraction and Co-NQR.^{10,11} However, probably due to the higher experimental resolution of single-crystal X-ray diffraction, we have discovered a lattice distortion to take place below T_0 , which is concluded to be a transition to a triclinic structure. The triclinic distortion is further modified in the AFM ordered phase. In addition, the structural domains can be selected by applying a magnetic field, suggesting that an electronic order exists behind and affects the magnetic anisotropy. These results pose a new question on the hidden ordered state of CeCoSi.

2. Experiment

Single crystals of CeCoSi were grown by Ce/Co eutectic flux method as described in Ref. 7. X-ray diffraction experiments were performed at BL-3A of the Photon Factory, KEK, Japan. A plate-shaped single-crystalline sample with an as-grown c -plane surface, $1.5 \times 2.0 \text{ mm}^2$ in area and 0.3 mm in thickness, was mounted in a vertical field 8 Tesla cryomagnet by using Apiezon-N grease so that the c -axis was parallel to the horizontal scattering plane. The $(H, 0, L)$ and (H, H, L) scattering planes were selected by rotating the sample about the c -axis, where the field direction was along $[010]$ and $[\bar{1}10]$, respectively. We used a two-dimensional Timepix area detector with 256×256 pixels at a pitch of $55 \mu\text{m}$, which covered approximately two degrees each for the horizontal (2θ) and vertical (χ) directions. The total intensity of the Bragg peak was measured by an oscillation method, where the crystal angle (θ) was rotated by approximately two degrees about the Bragg peak. We used an X-ray beam with a wavelength of 1.385 \AA (8.952 keV) in a nonresonant region. We also used a laboratory-based rotating anode X-ray source (Cu- $K\alpha$) and a two-axis diffractometer to measure the temperature (T) dependence of the lattice parameters between 3 K and 300 K for the same single crystal.

3. Results and Analysis

3.1 Temperature and magnetic-field dependences

Figure 2 shows the scattering angle (2θ) dependences of the intensity of the (0 0 8), (2 0 7), and (1 1 8) fundamental Bragg reflections at temperatures ranging from 3 K to 25 K. The original two dimensional data have been converted to the one dimensional 2θ dependence by integrating the pixel intensity along the vertical direction.¹⁹ As it is clearly observed, the (0 0 8) peak does not show any splitting and the peak position exhibits a smooth T -dependence with a minimum at 13 K.

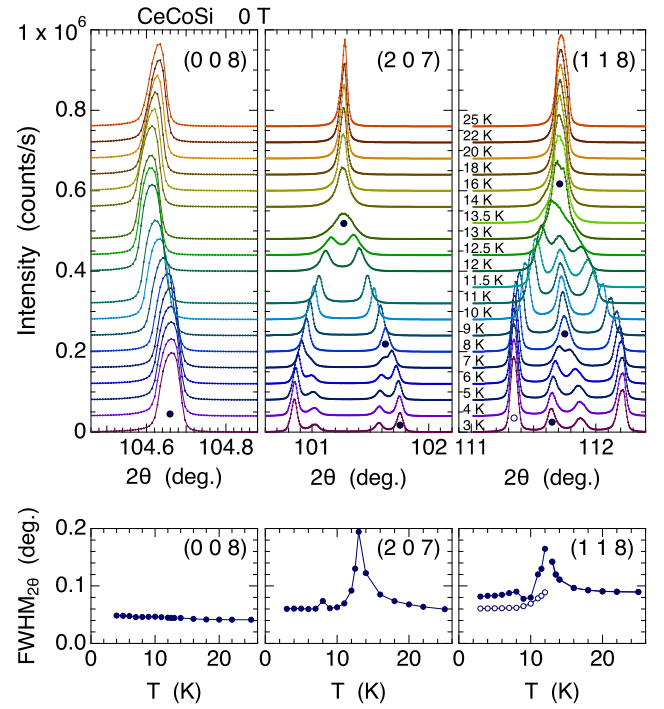


Fig. 2. (Color online) Top: Scattering angle dependences of the intensity of the (0 0 8), (2 0 7), and (1 1 8) Bragg reflections at zero field between 3 K and 25 K. Note the different scale of the horizontal axis for (0 0 8). Bottom: Temperature dependences of the full width at half maximum (FWHM) of the Bragg peak indicated by the mark (closed circle) in the top panels. For (1 1 8), the FWHM for another peak indicated by the open circle is also shown. The marks on the (2 0 7) and (1 1 8) peaks at 8 K and 13 K, below which the peak is split, represent that the peak is treated as a single peak in evaluating the FWHM at and above these temperatures.

The (2 0 7) and (1 1 8) peaks, on the other hand, exhibit clear splittings below 13 K. The (2 0 7) peak splits into two peaks below 13 K, both of which further split into two peaks below 8 K, which is slightly lower than T_N . The (1 1 8) peak splits into three peaks below 13 K and the central peak splits into two peaks below 8 K.

The T -dependences of the full width at half maximum (FWHM) of the Bragg peaks, obtained from the fits to multiple squared Lorentzian functions, are also shown in the bottom panels of Fig. 2. These are the FWHMs of the representative peak indicated by the mark in the top panels. For (0 0 8), the peak profiles at all temperatures were treated as a single peak. For (2 0 7) and (1 1 8), the profiles for $T \geq 13 \text{ K}$, as indicated by the marks (closed circle on the data at 13 K in the top panels), were treated as a single peak. The profiles for $8 \leq T \leq 12.5 \text{ K}$ were treated as double peaks for (2 0 7) and triple peaks for (1 1 8). For $T \leq 7 \text{ K}$ the profiles were treated as quadruple peaks. The broad profile at 12.5 K for (1 1 8) was excluded from the FWHM analysis because it was difficult to resolve the three peaks. The FWHM of the (0 0 8) peak does not exhibit any noticeable anomaly since no splitting takes place. The FWHM of the (2 0 7) and (1 1 8) peaks, by contrast, exhibits a significant increase with decreasing T toward 13 K, implying an increase in the structural instability. Below the transition at 13 K, the width decreases with decreasing T and again exhibits a weak increase at 8 K.

Figure 3 shows the T -dependence of the peak position, L in (H, K, L) , of the (0 0 8) reflection in the reciprocal lattice

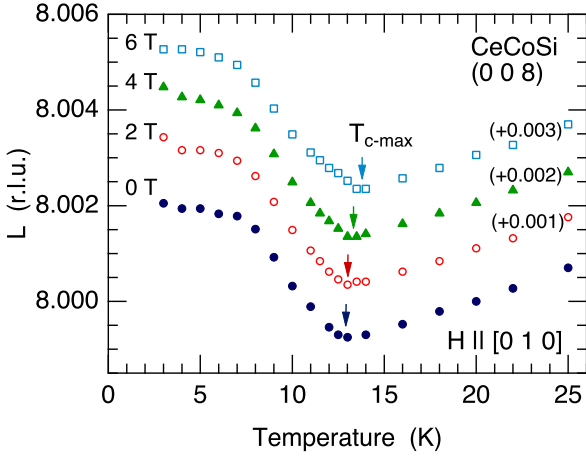


Fig. 3. (Color online) Temperature dependence of the peak position of the (0 0 8) reflection, L in (H, K, L) , expressed in the reciprocal lattice unit of the tetragonal lattice. The temperature indicated by the arrow is named as T_{c-max} , where the c -axis lattice parameter takes the maximum. Magnetic fields are applied along the [0 1 0] direction. The data for 2 T, 4 T, and 6 T are shifted by 0.001, 0.002, and 0.003, respectively. The reciprocal lattice is defined so that $L = 8$ at 20 K.

of the original tetragonal unit cell. Since the minimum in L corresponds to the maximum in the lattice parameter c , the temperature at which L takes the minimum is named as T_{c-max} . When a magnetic field is applied along [0 1 0], T_{c-max} shifts to higher temperatures. It is noted that the specific heat of the sample used in this study shows the anomaly of T_0 at 13 K.¹⁹⁾ These results show that T_{c-max} corresponds to T_0 .

It is also anomalous that the lattice parameter c decreases with increasing temperature above T_0 , indicating a negative thermal expansion. This unusual behavior persists up to the room temperature.¹⁹⁾ The lattice parameter a , on the other hand, exhibits a normal T -dependence as it increases almost linearly with T . It is noted that the relation $\Delta c/c \approx -0.75\Delta a/a$ holds above T_{c-max} . In view of the two-dimensional nature of the crystal structure, where the rigid Co-Si layers seem to be weakly coupled along the c -axis,⁷⁾ the negative thermal expansion along the c -axis suggests that the total thermal expansion is mostly determined by the in-plane bonding; i.e., when the ab -plane contracts, the lattice consequently expands along the c -axis. This may be associated with the distinctive pressure dependence of c/a in CeCoSi.^{20,21)}

Figure 4(a) shows the T -dependences of the peak position, L in (H, K, L) , of the (2 0 7) reflection in magnetic fields applied along the [0 1 0] direction.¹⁹⁾ As demonstrated in Fig. 2, the (2 0 7) peak exhibits a clear splitting below $T_0 = 13$ K at zero field into two peaks, indicating an occurrence of a structural transition at T_0 . In magnetic fields, the structural transition temperature, which we name as T_{s1} , decreases with increasing the field. On the other hand, T_{c-max} ($= T_0$) increases with increasing the field, which is also observed as a minimum in L in (2 0 7). Below T_{c-max} the peak position L increases with decreasing T down to T_{s1} , where the peak splits into two. This result shows that T_{s1} separates from T_0 in magnetic fields, whereas they coincide at zero field. As shown in Fig. 4(b) for a representative peak, the FWHM increases with decreasing T toward T_{s1} , implying an increase in the structural instability at all magnetic fields (see supplemental ma-

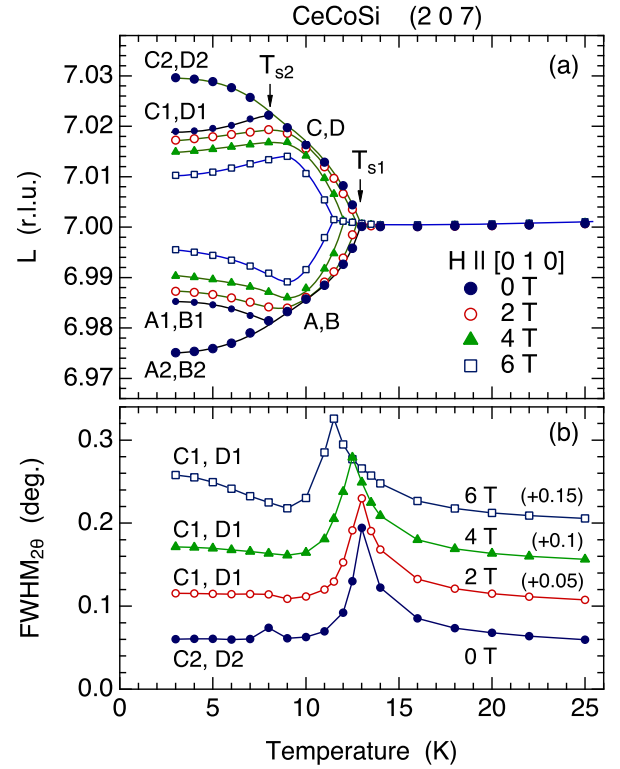


Fig. 4. (Color online) (a) Temperature dependences of the peak position of the (2 0 7) reflection, L in (H, K, L) , expressed in the reciprocal lattice unit of the tetragonal lattice. Magnetic fields are applied along the [0 1 0] direction. The labels represent the domain assignments shown in Fig. 8. (b) Temperature dependences of the FWHM for the peak corresponding to the structural domain represented by the label. The data for 2 T, 4 T, and 6 T are shifted by the value shown in the parentheses

terial for the original peak profile).¹⁹⁾ After exhibiting a sharp peak at T_{s1} , the FWHM decreases toward the resolution limit of 0.05° for (2 0 7) with decreasing T .

To deduce the FWHM, the peak profile at T_{s1} (e.g. 13 K for 0 T) is treated as a single peak and that just below T_{s1} (e.g. at 12.5 K for 0 T) is treated as double peaks. It is noted that, at 0 T for example, the FWHM $\sim 0.2^\circ$ at 13 K is almost equal to the peak split at 12.5 K. It is therefore not possible to distinguish experimentally whether the peak profile at 13 K is double peaked with a split by $\sim 0.1^\circ$ or is single peaked with a FWHM of $\sim 0.2^\circ$ (both can fit the data). The purpose of plotting the FWHM in this paper, whichever the case may be, is to show and emphasize the tendency of the peak splitting, i.e. the existence of lattice instability at the structural transition.

In the AFM ordered phase, the double peak splits into four peaks at zero field, indicating an occurrence of a second structural transition. Since the transition temperature of 8 K appears to be slightly lower than T_N , we named the temperature as T_{s2} to distinguish it from T_N . At $T_{s2} = 8$ K, the FWHM of the Bragg peak exhibits a weak increase at 0 T. As explained above, this suggests a structural instability taking place below $T_N = 9.4$ K before it is fixed below $T_{s2} = 8$ K and the peak starts to split. It is also noted that the T -dependence of the peak split at 0 T shown in Fig. 4(a) seems to close at 8 K by extrapolation and not at 9 K. This point will be discussed later in Sec. 3.3.

By applying a field of 2 T, the peak splitting below T_{s2} soon

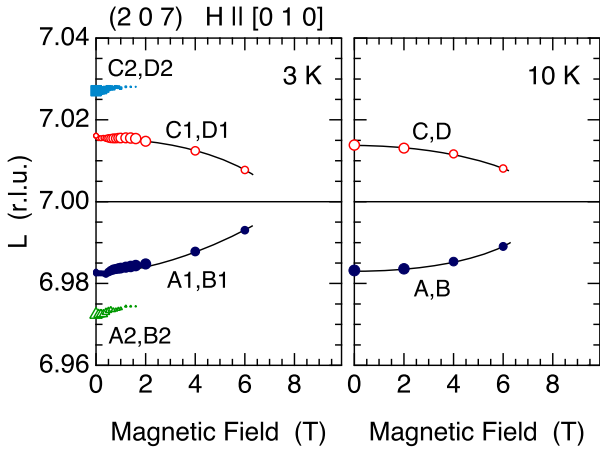


Fig. 5. (Color online) Magnetic field dependence of the peak position of the (2 0 7) reflection, L in (H, K, L) , at 3 K and 10 K, expressed in the reciprocal lattice unit of the tetragonal lattice. The size of the marks represent the peak intensity.

disappears because the structural domains corresponding to the inner peaks are selected. The domain selection below T_N above 2 T, or in other words a structural transition across T_N , is observed as the maximum in the peak split at around 9 K, which seems to coincide with T_N . The FWHM does not exhibit a cusp anomaly in magnetic fields above 2 T after the preferable domains are selected. With respect to the data at 6 T, the FWHM increases with decreasing T down to the lowest temperature of 3 K. This reflects the approach to another boundary at around 8 T as explained next.

Magnetic field dependence of the peak position L of the (2 0 7) reflection for $H \parallel [0 1 0]$ is shown in Fig. 5.¹⁹⁾ At 3 K, the outer peaks soon disappear by applying a field of ~ 1 T and the intensity is transferred to the inner peaks, indicating that the preferable structural domains are selected by the magnetic field. The intensity of the outer peaks almost disappear at 2 T. The width of the split between the inner peaks gradually decrease above 2 T. The split peaks are expected to merge back into the original central peak at around 8 T. This is also the case at 10 K. The critical field at 3 K seem to be lower than that at 10 K.

Next, we rotated the crystal by 45° , changed the scattering plane to (H, H, L) , and investigated the (1 1 8) reflection. Figure 6(a) shows the T -dependence of the peak position, L in (H, K, L) , of the (1 1 8) reflection in magnetic fields applied along the $[\bar{1} 1 0]$ direction. First, at zero field, the (1 1 8) peak splits into three below T_{s1} and the central peak splits into two below T_{s2} . In magnetic fields, the split outer peaks become weak because of the domain selection.¹⁹⁾ At 6 T, it was difficult to determine the (H, K, L) -index because the peak intensity was too weak. From the T -dependence of the peak split at 2 T, T_{s1} does not seem to change by the field, which is different from the result of (2 0 7) for $H \parallel [0 1 0]$. On the other hand, the peak position L of the central peak exhibits a minimum at T_0 and increases with decreasing T below T_0 . It seems difficult to distinguish whether T_{s1} deviates from T_0 or not from the peak split because the domain population is mostly transferred to the central peak and the intensities of the split peaks become very weak above 4 T.

Figure 6(b) shows the T -dependences of the FWHM of the

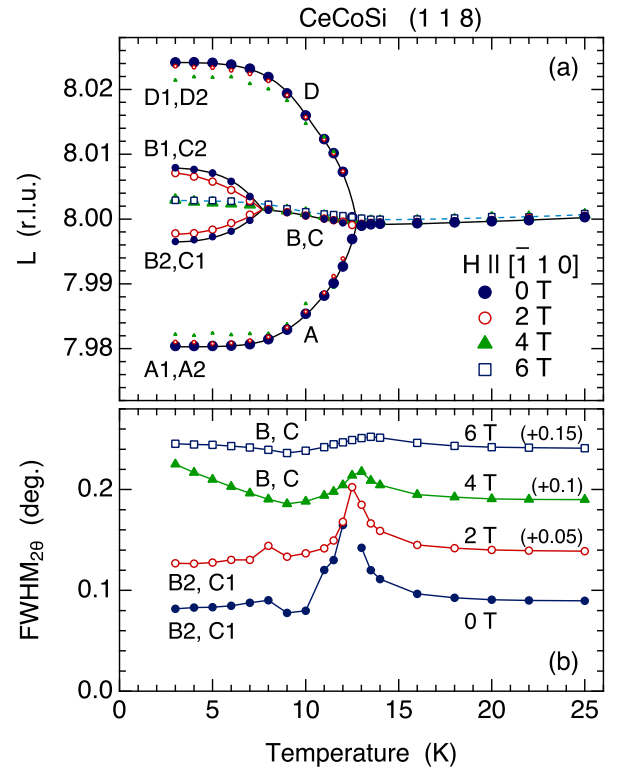


Fig. 6. (Color online) (a) Temperature dependences of the peak position of the (1 1 8) reflection, L in (H, K, L) , expressed in the reciprocal lattice unit of the tetragonal lattice. Magnetic fields are applied along the $[\bar{1} 1 0]$ direction. The labels represent the domain assignments shown in Fig. 8. (b) Temperature dependences of the FWHM for the peak corresponding to the structural domain represented by the label. The data for 2 T, 4 T, and 6 T are shifted by the value shown in the parentheses.

central peaks that remain up to high fields.¹⁹⁾ Although it was difficult to follow the field dependence of T_{s1} from the peak split as described above, the FWHM exhibits a cusp anomaly even at 6 T where the split peaks are difficult to observe. The increase in FWHM, reflecting the structural instability, strongly suggests that the transition at T_{s1} still exists even at 6 T and that T_{s1} increases with increasing the field, i.e., $T_{s1} = T_0$ for $H \parallel [\bar{1} 1 0]$. Since the increase in FWHM reflects the tendency of the peak splitting, the anomaly becomes weaker as the intensities of the split peaks transfer to the central peak due to the domain selection by the applied field. This is a different situation for $H \parallel [\bar{1} 1 0]$ than for $H \parallel [0 1 0]$ in Fig. 4(b). At $T_{s2} = 8$ K the FWHM again exhibits a weak cusp anomaly at 0 T and 2 T, reflecting the lattice instability taking place in the AFM phase. Above the phase boundary at 4 T, which is explained next, the cusp anomaly disappears. At the boundary of 4 T, the FWHM increases with decreasing T below 9 K, reflecting the increase in structural instability by approaching the phase boundary.

Magnetic field dependence of the peak position L of the (1 1 8) reflection for $H \parallel [\bar{1} 1 0]$ is shown in Fig. 7.¹⁹⁾ At 3 K, as for (2 0 7), the intensity of the outer peaks is rapidly transferred to the inner peaks at around 1 T, indicating the domain selection by the field. The width of the peak split between the inner peaks gradually decreases and the split peaks merge back into the central peak at 4 T. The intensity of the outer peaks weakly remains at 4 T, which further decreases at 6 T

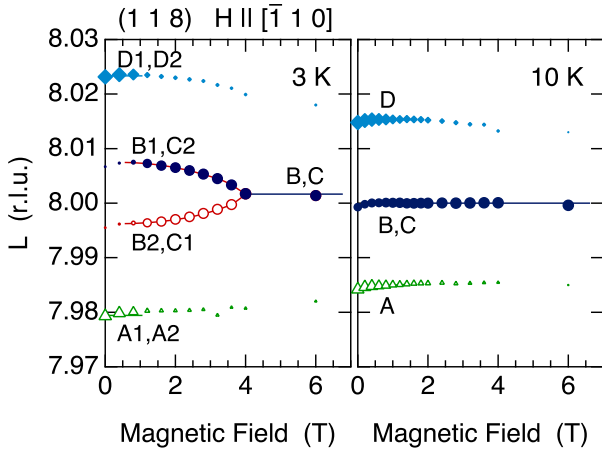


Fig. 7. (Color online) Magnetic field dependence of the peak position of the (1 1 8) reflection, L in (H, K, L) , at 3 K and 10 K, expressed in the reciprocal lattice unit of the tetragonal lattice. The size of the marks represent the peak intensity.

to a negligible level, but it still appears to remain finite. Also at 10 K, the intensity of the outer peak shows a steep decrease at around 1 T and a gradual decrease up to 4 T. The intensity still appears to remain finite even at 6 T. The decreased intensity is transferred to the central peak.

3.2 Triclinic distortion

Let us analyze the crystal structure at zero field to consistently explain the peak splitting of the (0 0 8), (2 0 7), and (1 1 8) reflections shown in Figs. 3, 4, and 6, respectively. No splitting in the (0 0 8) reflection shows that the direction of the reciprocal lattice vector c^* does not change. The splitting of the (2 0 7) and (1 1 8) Bragg peaks into two and three along L , respectively, can be explained by considering that the c -axis tilts to the $[1 1 0]$ and the equivalent directions, consequently forming a monoclinic lattice. Finally, to explain the splitting of H , it is necessary to introduce different lattice parameters for a and b , indicating that the lattice is distorted to triclinic.¹⁹⁾ The distorted lattice in the temperature range $T_{s2} < T < T_{s1}$ is illustrated in Fig. 8(A) and its equivalent domains are shown in Figs. 8(B), (C), and (D). With respect to the domain-A at 10 K, the relative change in the lattice parameters with respect to those at 20 K are estimated to be $\Delta a/a = 5.0 \times 10^{-4}$, $\Delta b/b = -5.0 \times 10^{-4}$, and $\Delta c/c = -2.2 \times 10^{-4}$. The triclinic angles are $\alpha = 89.64^\circ$, $\beta = 89.64^\circ$, and $\gamma = 90.0^\circ$. The volume contraction is calculated to be $\Delta V/V = -2.6 \times 10^{-4}$, which is consistent with fact that T_0 increases by applying an external pressure.^{5-7, 11)} Although the angle γ is not necessarily equal to 90° in the triclinic lattice, the deviation is too small (less than 0.05°) to determine within the accuracy of the present measurement. All the data were consistently explained by assuming $\gamma = 90.0^\circ$.

The peak split below T_{s2} can be explained by considering an additional tilt of the c -axis to the directions perpendicular to the first one below T_{s1} . For each domain from A to D, there arise two domains, which are named A1, A2, etc., resulting in eight domains in total. The peak assignments to these domains are given in Figs. 4, 5, 6, and 7.

In magnetic fields of $H \parallel [0 1 0]$, the A1, B1, C1, and D1 domains are selected and the A2, B2, C2, and D2 domains dis-

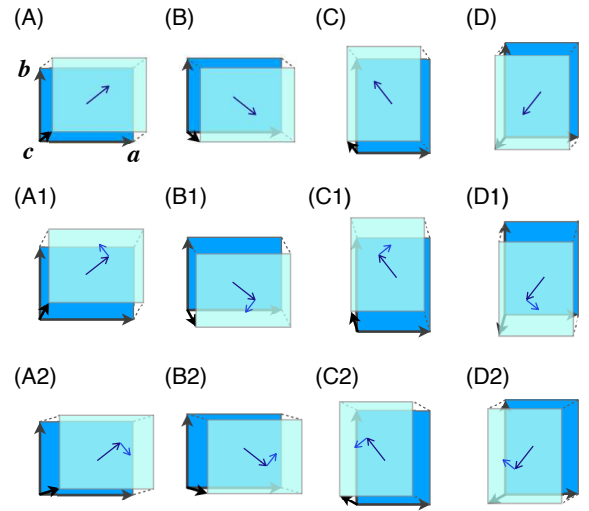


Fig. 8. (Color online) A model of the triclinic structure after the structural transition. A, B, C, and D represent the four types of structural domains below T_{s1} . The arrow on the upper ab -plane represents the direction of the shift of the plane from the tetragonal lattice. A1, A2 etc. are the domains below T_{s2} . The short arrow on the upper ab -plane represents the direction of the secondary shift of the plane below T_{s2} .

appear.¹⁹⁾ At 3 K in the AFM phase, the intensities of the outer peaks (A2, B2, C2, D2) rapidly decrease by applying a field of ~ 1 T and almost disappear at 2 T. The intensities transfer to the inner peaks (A1, B1, C1, D1). With further increasing the field, the width of the split between the inner peaks gradually decreases, and the peaks are expected to merge back into the original central peak at around 8 T.

In magnetic fields of $H \parallel [\bar{1} 1 0]$, the domains B and C are selected and the domains A and D disappear approximately at 1 T. At 3 K in the AFM phase, the width of the peak split between the inner peaks of the domains B and C gradually decrease and merge back into the central peak at 4 T. It is noted, however, as shown by the tiny marks in Figs. 6 and 7, the intensities of the outer peaks of the domains A and D weakly remain up to 4 T. Although they become very weak at higher fields, they still survive even at 6 T (see supplemental material). From these results of domain selection, we can see that the structural domains are preferred in which the tilt of the c -axis has more parallel component to the applied field. This is a common nature irrespective of the temperature above or below T_N .

3.3 Magnetic field vs temperature phase diagram

From the above results, we have constructed a phase diagram from the structural viewpoint. The result for $H \parallel [0 1 0]$ is shown in Fig. 9. First, the onset temperature of the hidden order, T_0 , is equal to $T_{c-\max}$ and increases with increasing the field. This is consistent with the previous reports.^{7, 8, 11)} Second, a structural transition takes place at T_{s1} , which is equal to T_0 at zero field and decreases with increasing the field. Below T_{s1} , the (2 0 7) peak splits into two peaks.

As shown in Fig. 4(b), the FWHM exhibits a significant increase at T_{s1} . This is considered to reflect an enhancement of the triclinic structural instability on approaching T_{s1} . At temperatures above T_{s1} , although the spatial and time average of the structure must still be tetragonal, or orthorhombic

in magnetic fields in a strict sense, short-ranged or instantaneous fluctuation of the triclinic phase is enhanced on approaching T_{s1} , where the phase transition finally takes place and the Bragg peak splits.

At zero field, the (2 0 7) peak further splits into four peaks below T_{s2} , where the triclinic structure is modified by the appearance of the AFM order. The result that T_{s2} appears to be lower than T_N by ~ 1 K at 0 T can possibly be considered as reflecting the similar kind of structural instability of the low- T triclinic phase, which becomes significant just below T_N on entering the AFM phase. For example, when the AFM order takes place in the triclinic domain-A, there can arise a structural fluctuation between the two domains of A1 and A2, which consequently results in a slightly lower transition temperature of T_{s2} than T_N . The enhanced instability is reflected in the weak increase in the FWHM at 8 K at 0 T as shown in Fig. 4(b).

Above 1 T, as represented by the horizontal dotted line, the preferable structural domains below T_N (A1, B1, C1, D1) are selected, leaving two peaks to remain. The two peaks are expected to vanish at around 8 T, which is expected to be connected to T_{s1} above T_N . When the preferable domains are selected above 1 T, a structural transition (or a crossover) from phase II ($T_0 > T > T_N$) to III ($T < T_N$) is observed at around 9 K, which is in agreement with T_N . This may be because the structural fluctuation is suppressed by selecting the preferable structural domain by the applied field.

The phase diagram for $H \parallel [\bar{1} 1 0]$ constructed from the available data, though not comprehensive yet, is shown in Fig. 10. For $H \parallel [\bar{1} 1 0]$, T_0 is almost equal to that for $H \parallel [0 1 0]$ as observed in the maximum of the lattice parameter c . The second structural transition at T_{s2} still exists even in a magnetic field of 2 T as shown in Fig. 6(a). This may be because the structural fluctuation remains in magnetic fields for $H \parallel [\bar{1} 1 0]$ even above the initial domain selection at 1 T. For example, when the AFM order takes place in the triclinic domain-B at 2 T, there remains a fluctuation between the domains B1 and B2, which causes the second structural transition at T_{s2} and causes the peak splitting within the preferred domain. We consider that this is reflected in the increase in the FWHM at T_{s2} as shown in Fig. 6(b) for 0 T and 2 T.

There is also a boundary at 4 T as observed in the disappearance of the peak split at 3 K in the central peak shown in Fig. 7. This boundary is also reflected in the increase in the FWHM with decreasing T below 9 K at 4 T as shown in Fig. 6(b). In magnetic fields above 4 T, the B and C structural domains are selected and the intensities from the A and D domains significantly decrease. It is noted that, since the central peak of the (1 1 8) reflection corresponding to the B and C domains does not split, it is not clear whether the B and C triclinic domains persist or they come back to the tetragonal structure, or an orthorhombic structure in a strict sense in magnetic fields.¹⁹⁾ We cannot distinguish the two possibilities. However, judging from the fact that the weak intensities from the A and D domains remain above 4 T, indicating the domain selection and not the change in the lattice type and the symmetry, it is inferred that the B and C domains continue to exist up to higher fields. In addition, also from the result that the FWHM of the central peak exhibits a cusp anomaly at T_0 at 4 T and 6 T, reflecting the peak split due to the appearance of the A and D domains, the transition from the tetragonal to

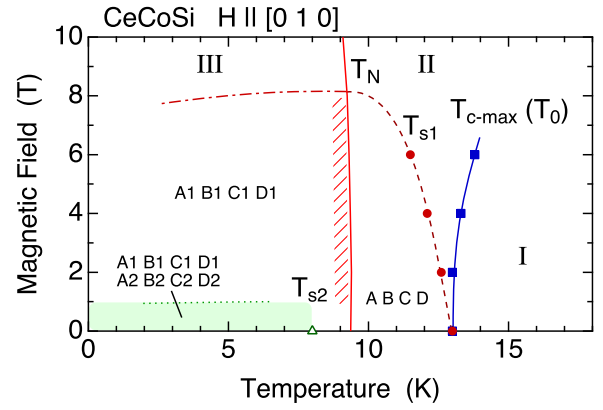


Fig. 9. (Color online) Magnetic-field vs temperature phase diagram of CeCoSi for $H \parallel [0 1 0]$ constructed from the results of (2 0 7) and (0 0 8) reflections. T_{c-max} represents the temperature where the lattice parameter c takes the maximum, which is equal to T_0 . Vertical solid line represents T_N taken from the literature.⁷⁾ T_{s1} and T_{s2} are the temperatures below which the (2 0 7) peak splits into two and four peaks, respectively. The dashed line connecting T_{s1} is a guide for the eyes. The horizontal dotted line at 1 T represents the boundary of domain selection. See Fig. 8 for the name of the triclinic domains. The shaded area around 9 K represents the structural crossover across T_N .

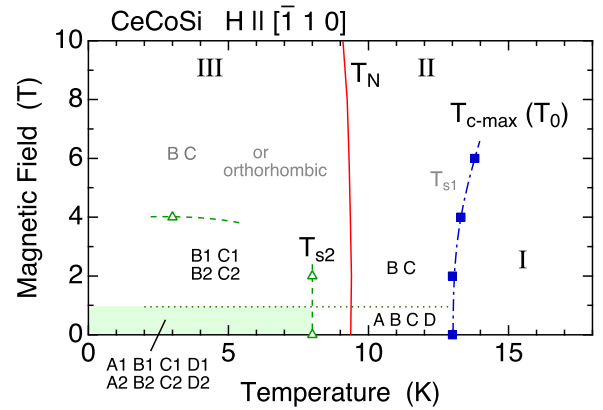


Fig. 10. (Color online) Magnetic-field vs temperature diagram for $H \parallel [\bar{1} 1 0]$ constructed from the results of (1 1 8) reflection. It has not been clarified whether the B and C triclinic domains persist up to high fields above 4 T with $T_{s1} = T_0$ or the high field phase is orthorhombic without structural transition at T_{s1} .

the triclinic domains of B and C is also likely to exist at high fields above 4 T. If this is the case, $T_{s1} = T_0$ is concluded for $H \parallel [\bar{1} 1 0]$.

However, since the main peak of the (1 1 8) reflection at the center above 4 T is unambiguously a single peak, from which we cannot extract any evidence for the triclinic distortion. If we neglect the tiny peaks for the A and D domains as residual signals, there arise also a possibility that the structure above 4 T for $H \parallel [\bar{1} 1 0]$ could be orthorhombic. In this case, the weak anomaly in FWHM at T_{s1} is regarded as extrinsic. It is concluded that T_{s1} does not exist above 4 T for $H \parallel [\bar{1} 1 0]$. These two possibilities above 4 T are written by gray letters in the phase diagram in Fig. 10. The phase diagram for $H \parallel [\bar{1} 1 0]$ needs to be studied in more detail, which must be different from that for $H \parallel [0 1 0]$.

4. Discussions

Since the magnetic field itself does not have a direct interaction with the lattice, there should be some magnetic anisotropy originating from the electronic system in the triclinic phase, through which the structural domains are manipulated. Such an example can be found in the domain switching in the hexagonal YbAl_3C_3 and DyAl_3C_3 , where the structural domains in the low temperature orthorhombic phase can be manipulated by the magnetic field even in the paramagnetic state probably through the very weak magnetic anisotropy.²²⁾ Also in the present case of CeCoSi , the magnetic anisotropy in the ab -plane is considered to be very small since the CEF ground state is nearly isotropic.¹⁰⁾ Although it is speculated that the ferroquadrupole order of $O_{yz} + O_{zx}$ corresponding to the triclinic distortion gives rise to such a magnetic anisotropy, it still requires further study if such an ordering could be possible by considering the inter-orbital hybridization due to the noncentrosymmetry.

If the lattice is uniformly distorted in the triclinic structure, probably with the space group $P\bar{1}$ where all the atoms are at the general $2i$ site, there should arise no splitting in the NQR spectrum, but with a shift below T_0 , which is consistent with the experimental observation. To explain the peak splitting in NMR in magnetic fields, on the other hand, it is necessary to take into account an antiferro-type induced moment at the Co site.¹¹⁾ Even if we simply consider a ferroquadrupole order for the structural transition, it is still necessary to consider some antiferro-type order taking place below T_0 .¹⁸⁾

Therefore, the phase transition at T_0 is still in question. It should be associated with the Ce- $4f$ and a Ce-Ce interaction, possibly of nonmagnetic origin involving some orbital nature, since the order is fragile to La substitution.⁶⁾ In particular, the relation with the triclinic distortion is mysterious. For $H \parallel [010]$, T_0 and T_{s1} separate with increasing the field. The temperature region $T_{s1} < T < T_0$ is a purely hidden ordered phase without triclinic distortion, but with a lattice contraction along the c -axis and with some antiferro-type order of orbital nature. We note that the phase boundary at T_{s1} in magnetic fields has also been revealed recently by the bulk property measurements.²³⁾

One of the possibilities of the crystal structure of the purely hidden ordered phase for $H \parallel [010]$, which is induced by the underlying electronic order, could be a monoclinic one with the space group $P112/n$ (No. 13), a subgroup of an orthorhombic space group $Pmnm$ (No. 59), where $Pmnm$ is a subgroup of the tetragonal $P4/nmm$ (No. 129).¹⁹⁾ Although there has been no experimental evidence for the symmetry lowering from tetragonal to orthorhombic in the paramagnetic phase above T_0 , it may be assumed that the symmetry of the crystal is reduced to orthorhombic in a magnetic field applied along the $[010]$ direction. A possible consequence of the antiferro-type hidden order at T_0 could be an O_{xy} -type ferroquadrupole order, resulting in the symmetry lowering from orthorhombic to monoclinic. Since no peak splitting is observed in the region $T_{s1} < T < T_0$, the monoclinic distortion is expected to be negligibly small. In this phase, the c -axis is still perpendicular to the ab -plane. The O_{yz} and O_{zx} moments are induced below T_{s1} with the reduction to $P\bar{1}$. In our observation, the transition at T_0 is only reflected in the maximum of the c -axis lattice parameter. At zero field, this electronic order

and the triclinic distortion to $P\bar{1}$, allowing the O_{yz} and O_{zx} moments, take place simultaneously by skipping the monoclinic phase. For $H \parallel [\bar{1}10]$, we start from $Cmme$ (No. 67), where the orthorhombic axis is parallel to the field. In this case, the hidden order immediately induces the O_{yz} and O_{zx} moments and the tilt of the c -axis, resulting in the reduction to $P\bar{1}$ at $T < T_0$.

With respect to the possibility of quadrupole order, we note a recent article reporting a nonmagnetic phase transition at $T_0 = 0.4$ K in CeRh_2As_2 with the CaBe_2Ge_2 -type structure.^{24,25)} CeCoSi and CeRh_2As_2 , with the same space group $P4/nmm$, share a similar structural feature, where the site symmetry $4mm$ of Ce ($2c$ site) lacks the inversion symmetry but the crystal is globally centrosymmetric with an inversion center at the midpoint of the two Ce atoms in the unit cell. The transition at $T_0 = 0.4$ K is proposed to be a quadrupole density wave state, involving the conduction electrons through c - f hybridization. However, since the $\Gamma_7^{(1)}$ doublet CEF ground state and the Γ_6 first excited state at $\Delta_{\text{CEF}} \sim 30$ K are well separated, no quadrupolar degree of freedom is expected to remain at 0.4 K. A *metaorbital* transition is proposed to be a possible scenario of this ordering, where the CEF excited state is incorporated through a relatively strong hybridization with a Kondo temperature $T_K \sim 30$ K as high as the CEF splitting.^{25,26)} Since the Kondo temperature of CeCoSi , with a localized $4f$ state, is expected to be much lower than that of CeRh_2As_2 , this scenario may not be applicable. However, the ratio of T_0 to Δ_{CEF} of CeCoSi ($= 12$ K / 120 K) is much larger than that of CeRh_2As_2 ($= 0.4$ K / 30 K). If we take into account the orbital dependent hybridization, i.e., if the hybridization of the CEF excited state is stronger than that of the ground state, the quadrupole order by incorporating the CEF excited state could be a possible scenario also in CeCoSi .

Another point worth noting with respect to the structural transition of CeCoSi at T_0 above the AFM order is the similar anomaly reported in $\text{CeCo}_{1-x}\text{Fe}_x\text{Si}$.^{27,28)} The increase in the transition temperature by applying a magnetic field is reminiscent of the T_0 anomaly in CeCoSi and seems to be pronounced by Fe substitution, although the anomaly is broadened. To explain this unusual transition, a phenomenological thermodynamic theory was presented considering the magnetoelastic free energy.²⁹⁾ The theory well explains the field dependences of the structural transitions at T_N and T_0 , suggesting the importance of magnetoelastic coupling through the $4f$ quadrupole moments.

A similarity with the structural transition at 13.5 K in CePd_2Al_2 with the CaBe_2Ge_2 -type structure is also noteworthy.³⁰⁾ The transition temperature increases to ~ 50 K by applying a pressure of 3 GPa. The resistivity exhibits a step-like increase reminiscent of a gap opening as in CeCoSi . At ambient pressure, the symmetry lowering from tetragonal $P4/nmm$ to orthorhombic $Cmme$ at 13.5 K is accompanied by a significant anomalies in specific heat, magnetic susceptibility, and resistivity, which are much more pronounced than those in CeCoSi possibly because the lattice distortion of $\sim 1\%$ is much larger. The $4f$ entropy is expected to be involved in this structural transition through a magnetoelastic coupling as demonstrated by the formation of bound states between phonons and CEF excitations.^{31,32)} The weak anomaly at T_0 in CeCoSi may suggest that such effect is weaker than in CePd_2Al_2 .

5. Summary

In summary, we have studied the hidden ordered phase of CeCoSi by single-crystal X-ray diffraction in magnetic fields. The anomaly at T_0 is reflected in the maximum of the c -axis lattice parameter. At zero field, a structural transition to the triclinic lattice occurs simultaneously with the hidden order at T_0 . For $H \parallel [0\ 1\ 0]$ (equivalent to $[1\ 0\ 0]$), the temperature of the structural transition, T_{s1} , separates from T_0 and decreases with increasing the field, leaving the purely hidden ordered state without triclinic distortion to exist between T_{s1} and T_0 . A second lattice distortion occurs below T_{s2} , which is slightly lower than T_N , leading to a modification of the triclinic lattice reflecting the antiferromagnetic order. The preferred structural domains are selected by a weak magnetic field of 1 T. The triclinic distortion disappears at high fields above 8 T. We also studied the structural transitions for $H \parallel [\bar{1}\ 1\ 0]$ and showed that the phase diagram is much different from that for $H \parallel [0\ 1\ 0]$. These results strongly suggest that some electronic order of, e.g, a ferroquadrupole, exists behind and gives rise to a weak magnetic anisotropy in the triclinic phase. However, the origin of the hidden ordered phase, possibly with an antiferro-type order parameter, is still in mystery.

Acknowledgements The authors acknowledge valuable discussions with H. Harima, T. Tayama, H. Hidaka, H. Kotegawa, and M. Manago. This work was supported by JSPS KAKENHI Grants No. JP17K05130, 18H03683, JP20H04458, and No. JP20H01854. The synchrotron experiments were performed under the approval of the Photon Factory Program Advisory Committee (No. 2020G034). The temperature dependences of the lattice parameters from 3 K to 300 K were measured with an X-ray diffractometer (Cu-K α) of N-BARD, Hiroshima University.

- 1) Y. Kuramoto, H. Kusunose, and A. Kiss, *J. Phys. Soc. Jpn.* **78**, 072001 (2009).
- 2) S. Hayami, M. Yatsushiro, Y. Yanagi, and H. Kusunose, *Phys. Rev. B* **98**, 165110 (2018).
- 3) M.-T. Suzuki, T. Nomoto, R. Arita, Y. Yanagi, S. Hayami, and H. Kusunose, *Phys. Rev. B* **99**, 174407 (2019).
- 4) B. Chevalier, S. F. Matar, J. Sanchez Marcos, and J. Rodriguez Fernandez, *Physica B: Condensed Matter* **378-380**, 795 (2006).
- 5) E. Lengyel, M. Nicklas, N. Caroca-Canales, and C. Geibel, *Phys. Rev. B* **88**, 155137 (2013).
- 6) H. Tanida, Y. Muro, and T. Matsumura, *J. Phys. Soc. Jpn.* **87**, 023705 (2018).
- 7) H. Tanida, K. Mitsumoto, Y. Muro, T. Fukuhara, Y. Kawamura, A. Kondo, K. Kindo, Y. Matsumoto, T. Namiki, T. Kuwai, and T. Matsumura, *J. Phys. Soc. Jpn.* **88**, 054716 (2019).
- 8) H. Tanida, K. Mitsumoto, Y. Muro, T. Fukuhara, Y. Kawamura, A. Kondo, K. Kindo, Y. Matsumoto, T. Namiki, T. Kuwai, and T. Matsumura, *JPS Conf. Proc.* **30**, 011156 (2020).
- 9) K. Momma and F. Izumi, *J. Appl. Crystallogr.* **44**, 1272 (2011).
- 10) S. E. Nikitin, D. G. Franco, J. Kwon, R. Bewley, A. Podlesnyak, A. Hoser, M. M. Koza, C. Geibel, and O. Stockert, *Phys. Rev. B* **101**, 214426 (2020).
- 11) M. Manago, H. Kotegawa, H. Tou, H. Harima, and H. Tanida, *J. Phys. Soc. Jpn.* **90**, 023702 (2021).
- 12) Y. Kawarasaki, T. Matsumura, M. Sera, and A. Ochiai, *J. Phys. Soc. Jpn.* **80**, 023713 (2011).
- 13) H. Takaguchi, Y. Hayashi, T. Matsumura, K. Umeo, M. Sera, and A. Ochiai, *J. Phys. Soc. Jpn.* **84**, 044708 (2015).
- 14) Y. Hayashi, S. Takai, T. Matsumura, H. Tanida, M. Sera, K. Matsubayashi, Y. Uwatoko, and A. Ochiai, *J. Phys. Soc. Jpn.* **85**, 034704 (2016).
- 15) A. Yamamoto, J. Takeda, T. Koyama, T. Mito, S. Wada, I. Shiroani, and C. Sekine, *Phys. Rev. B* **70**, 220402 (2004).
- 16) A. Oyamada, S. Maegawa, T. Goto, K. Hashi, and H. Kitazawa, *J. Phys. Soc. Jpn.* **73**, 1953 (2004).
- 17) M. Yatsushiro and S. Hayami, *J. Phys. Soc. Jpn.* **89**, 013703 (2020).
- 18) M. Yatsushiro and S. Hayami, *Phys. Rev. B* **102**, 195147 (2020).
- 19) (Supplemental Material) The following pieces of information are provided online. (S1) The original two dimensional data and the process of integration. (S2–4) The detailed T -dependences of the peak profiles (2θ dependences) and the peak widths of the (0 0 8), (2 0 7) and (1 1 8) reflections in magnetic fields. (S5–7) The magnetic-field dependences of the peak profiles of the (2 0 7) and (1 1 8) reflections at fixed temperatures of 3 K and 10 K. (S8–9) The T -dependences of the peak position H in (H, K, L) for the (2 0 7) and (1 1 8) reflections. (S10) The specific heat of the sample used in this study. (S11) The T -dependences of the lattice parameters a, c , and the unit cell volume up to the room temperature. (S12) Group-subgroup relations from tetragonal $P4/nmm$ to triclinic $P\bar{1}$ for the present case in CeCoSi.
- 20) Y. Kawamura, H. Tanida, R. Ueda, J. Hayashi, K. Takeda, and C. Sekine, *J. Phys. Soc. Jpn.* **89**, 054702 (2020).
- 21) Y. Kawamura *et al.*, to be submitted.
- 22) T. Matsumura, Y. Hayashi, S. Takai, T. Otsubo, S. Matsuda, and A. Ochiai, *J. Phys. Soc. Jpn.* **84**, 114712 (2015).
- 23) H. Hidaka *et al.*, to be submitted.
- 24) S. Khim, J. F. Landaeta, J. Banda, N. Bannor, M. Brando, P. M. R. Brydon, D. Hafner, R. K uchler, R. Cardoso-Gil, U. Stockert, A. P. Mackenzie, D. F. Agterberg, C. Geibel, and E. Hassinger, *Science* **373**, 1012 (2021).
- 25) D. Hafner, P. Khanenko, E. O. Eljaouhari, R. K uchler, J. Banda, N. Bannor, T. L uhmann, J. F. Landaeta, S. Mishra, I. Sheikin, E. Hassinger, S. Khim, C. Geibel, G. Zwicky, and M. Brando, *Phys. Rev. X* **12**, 011023 (2022).
- 26) K. Hattori, *J. Phys. Soc. Jpn.* **79**, 114717 (2010).
- 27) J. G. Sereni, M. G. Berisso, D. Betancourth, V. F. Correa, N. C. Canales, and C. Geibel, *Phys. Rev. B* **89**, 035107 (2014).
- 28) V. F. Correa, D. Betancourth, J. G. Sereni, N. Caroca Canales, and C. Geibel, *J. Phys.: Condens. Matter* **28**, 346003 (2016).
- 29) W. G. C. Oropesa, V. F. Correa, J. G. Sereni, D. J. Garcia, and P. S. Cornaglia, *J. Phys.: Condens. Matter* **30**, 295803 (2018).
- 30) M. Klicpera, P. Dole al, J. Prokle ska, J. Prchal, and P. Javorsk y, *J. Alloys Compd.* **639**, 51 (2015).
- 31) L. C. Chapon, E. A. Goremychkin, R. Osborn, B. D. Rainford, and S. Short, *Physica B* **378-380**, 819 (2006).
- 32) M. Klicpera, M. Boehm, P. Dole al, H. Mutka, M. M. Koza, S. Rols, D. T. Adroja, I. Puente Orench, J. Rodr guez-Carvajal, and P. Javorsk y, *Phys. Rev. B* **95**, 085107 (2017).

Supplemental Material

Structural Transition in the Hidden Ordered Phase of CeCoSi

T. Matsumura, S. Kishida, M. Tsukagoshi, Y. Kawamura, H. Nakao, and H. Tanida

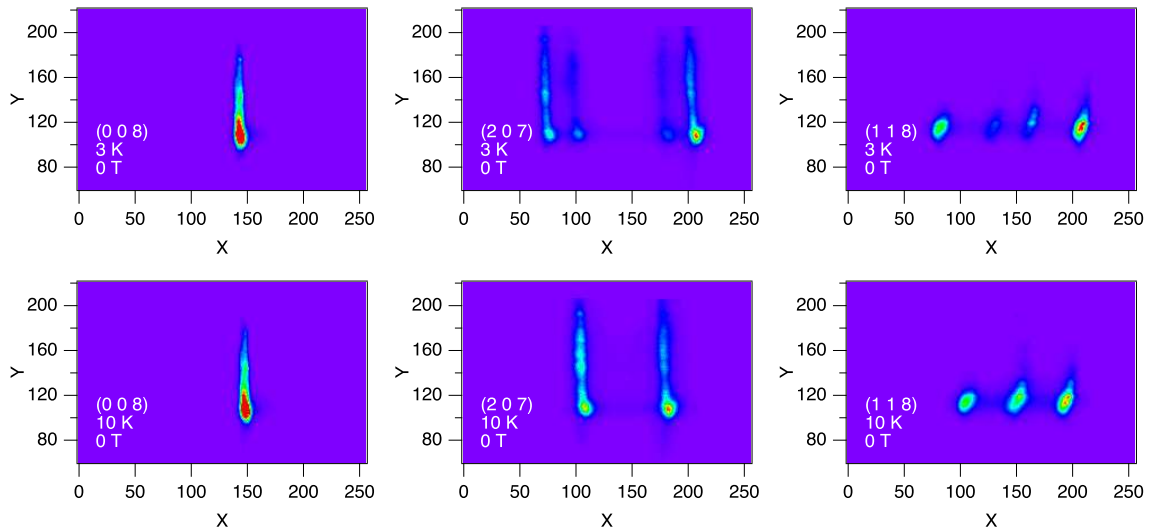


Fig. S1. X-ray oscillation photographs of the (0 0 8), (2 0 7), and (1 1 8) reflections at 3 K and 10 K at zero field. X and Y represent the pixel number of the detector. The intensity sum along Y between 90 and 130 were used to obtain the one dimensional 2θ dependence of the intensity (Fig. 2 in the main text. Figs. S2, S3, S4, S5, S6, and S7 in the supplemental material). One pixel along X corresponds to the 2θ angle of 0.0069° . The crystal angle (θ) was rotated by approximately two degrees about the Bragg peak. The θ -scan was also performed to determine the peak position and deduce the (H, K, L) index of the split peaks (Figs. 3, 4, 5, 6, and 7 in the main text. Figs. S8 and S9 in the supplemental material).

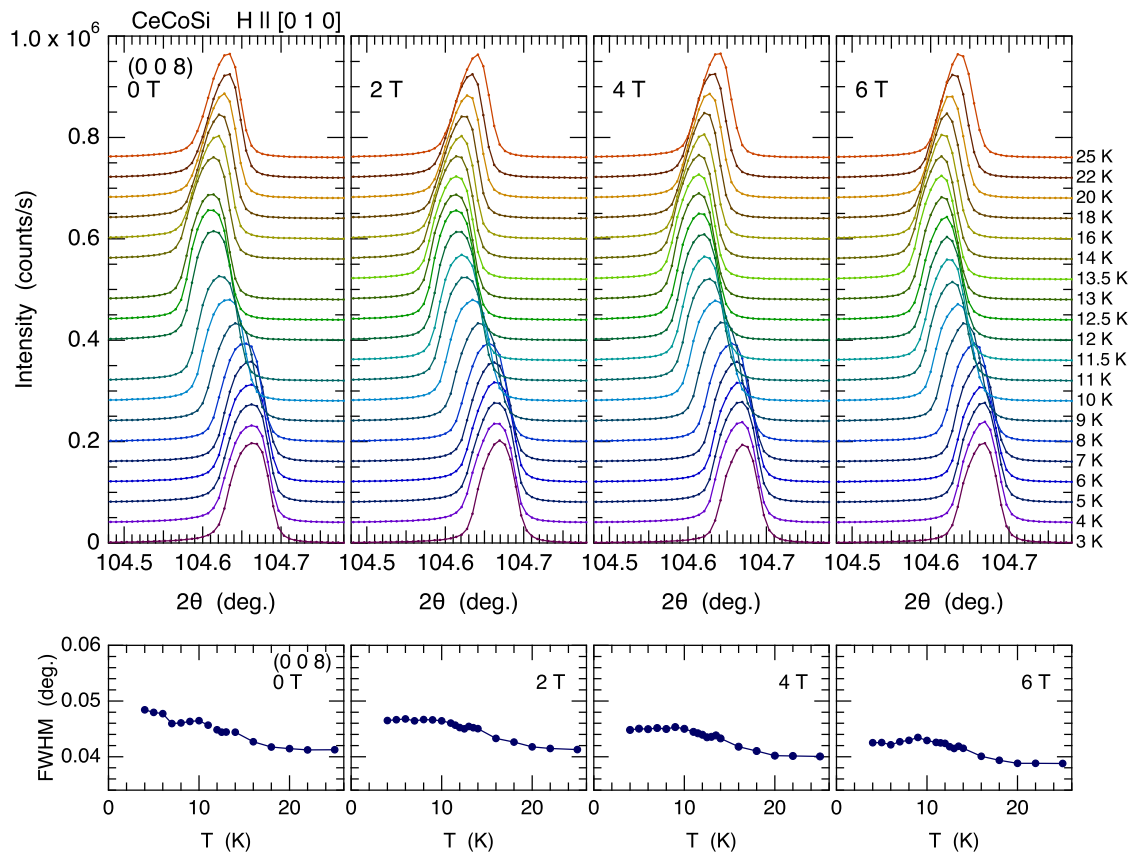


Fig. S2. (top) Scattering angle (2θ) dependences of the intensity of the (0 0 8) reflection in magnetic fields of 0 T, 2 T, 4 T, and 6 T applied along [0 1 0]. The T -dependences of L in (H, K, L) for (0 0 8) shown in Fig. 3 in the main text are obtained from the peak positions of these data. (bottom) T -dependences of the full width at half maximum (FWHM) of the Bragg peak obtained from the fit with a squared Lorentzian function. For (0 0 8), no cusp anomaly is observed in the FWHM, except for the gradual variation in slope at around 15 K.

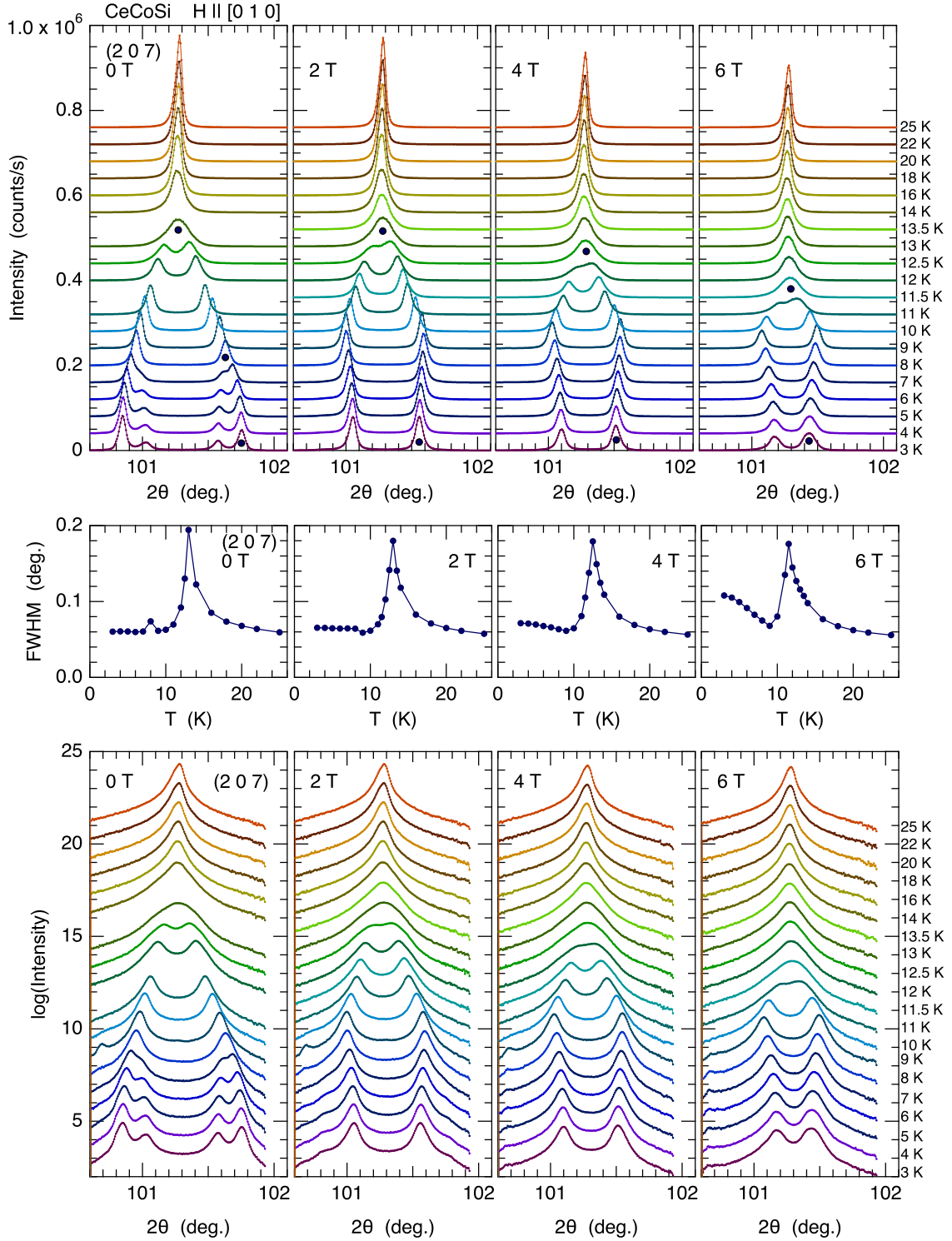


Fig. S3. (top) Scattering angle (2θ) dependences of the intensity of the (2 0 7) reflection in magnetic fields of 0 T, 2 T, 4 T, and 6 T applied along [0 1 0]. The T -dependences of L in (H, K, L) for (2 0 7) shown in Fig. 4 in the main text are obtained from the peak positions of these data. (middle) T -dependences of the full width at half maximum (FWHM) of the Bragg peak obtained from the fit with multiple squared Lorentzian functions. The FWHM is shown for the peak indicated by the mark (closed circle) in the top panels. The peak profiles for $T \geq 13$ K, 13 K, 12.5 K, and 11.5 K for 0 T, 2 T, 4 T, and 6 T, respectively, which are indicated by the marks in the top panels, were treated as a single peak. Below these temperatures the profiles were treated as double peaks. For 0 T, the profiles for $8 \leq T \leq 12.5$ K and for $T \leq 7$ K were treated as double peaks and four peaks, respectively, which are also indicated by the marks. (bottom) Scattering angle (2θ) dependences of the intensity plotted in a logarithmic scale.

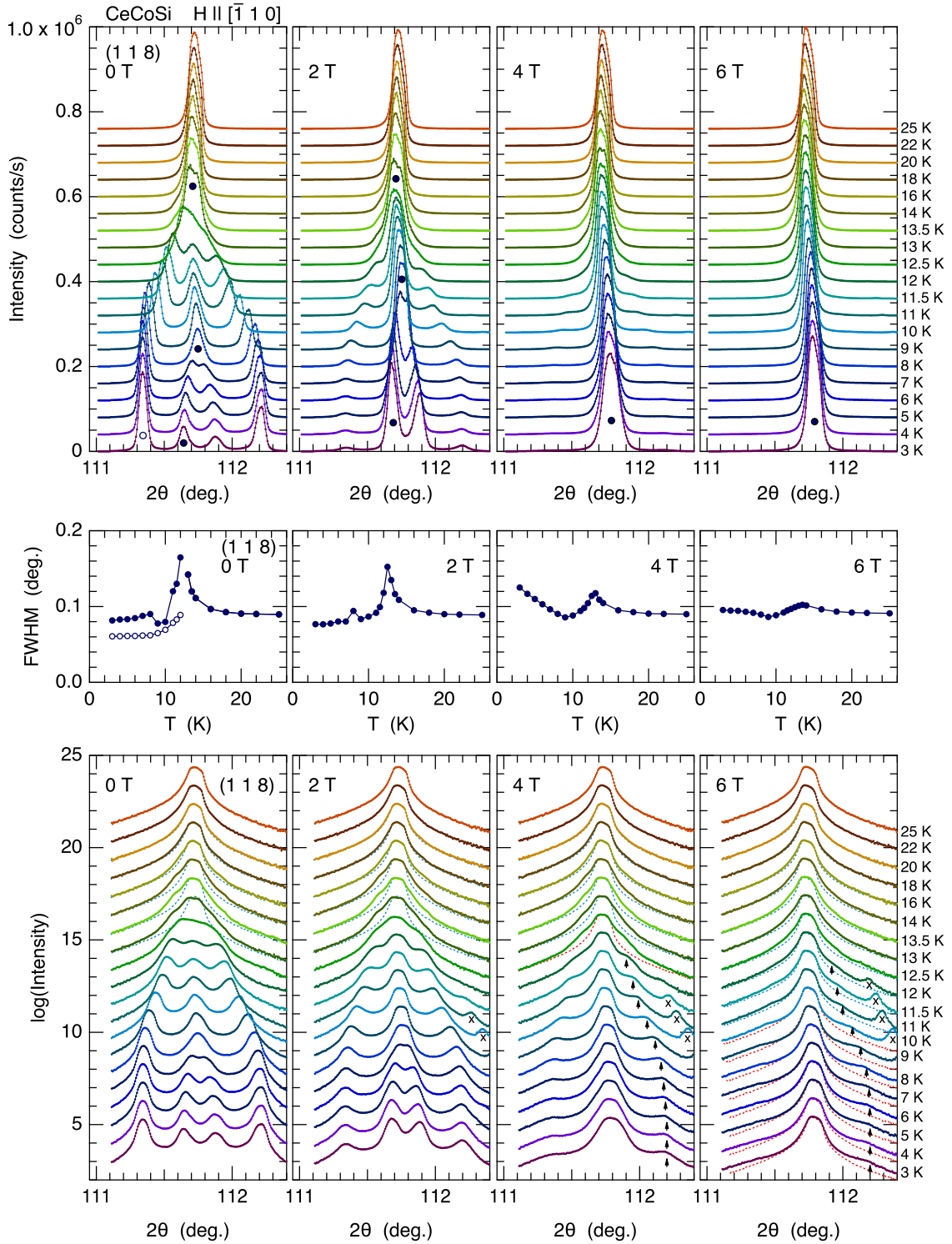


Fig. S4. (top) Scattering angle (2θ) dependences of the intensity of the (1 1 8) reflection in magnetic fields of 0 T, 2 T, 4 T, and 6 T applied along $[\bar{1} 1 0]$. (middle) T -dependences of the full width at half maximum (FWHM) of the Bragg peak obtained from the fit with multiple squared Lorentzian functions. The FWHM is shown for the peak indicated by the mark (closed circle) in the top panels. For 0 T, the FWHM for another peak (open circle) is also shown, which does not split below T_{Q2} . The peak profiles for $T \geq 13$ K for 0 T and 2 T, and all the profiles for 4 T and 6 T, were treated as a single peak as indicated by the marks in the top panels. For 0 T and 2 T, the profiles for $8 \leq T \leq 12.5$ K and for $T \leq 7$ K were treated as three peaks (one central and two outer peaks) and four peaks (two central and two outer peaks), respectively. The broad profile at 12.5 K for 0 T, which consists of three unresolved peaks, was excluded from the FWHM analysis. (bottom) Scattering angle (2θ) dependences of the intensity plotted in a logarithmic scale. The dashed lines are the profile at 25 K for comparison. The arrows in the panels of 4 T and 6 T indicate the positions of the weakly observed outer peaks. The x marks indicate the unidentified peaks.

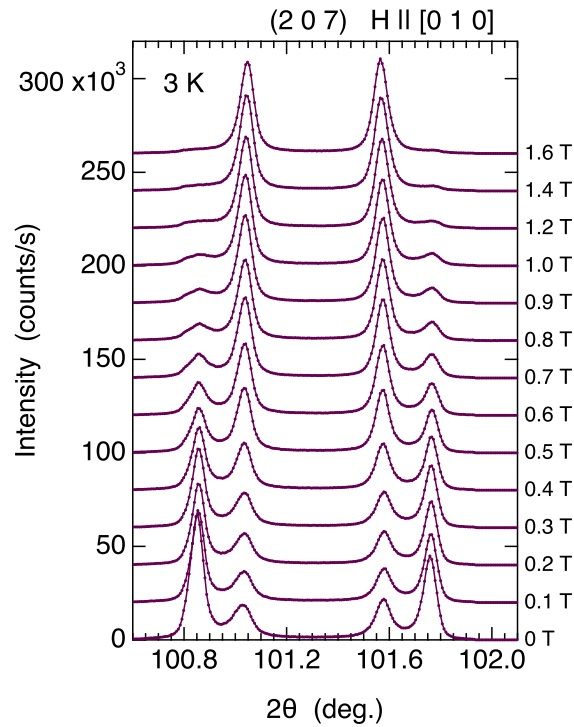


Fig. S5. Scattering angle (2θ) dependences of the intensity of the (2 0 7) reflection at 3 K in magnetic fields applied along [0 1 0]. The intensities of the outer peaks rapidly decrease by applying the field and almost disappear above 2 T. The intensities transfer from the outer peaks to the inner peaks. The field dependence of L in (H, K, L) for (2 0 7) shown in Fig. 5 in the main text are obtained from these data.

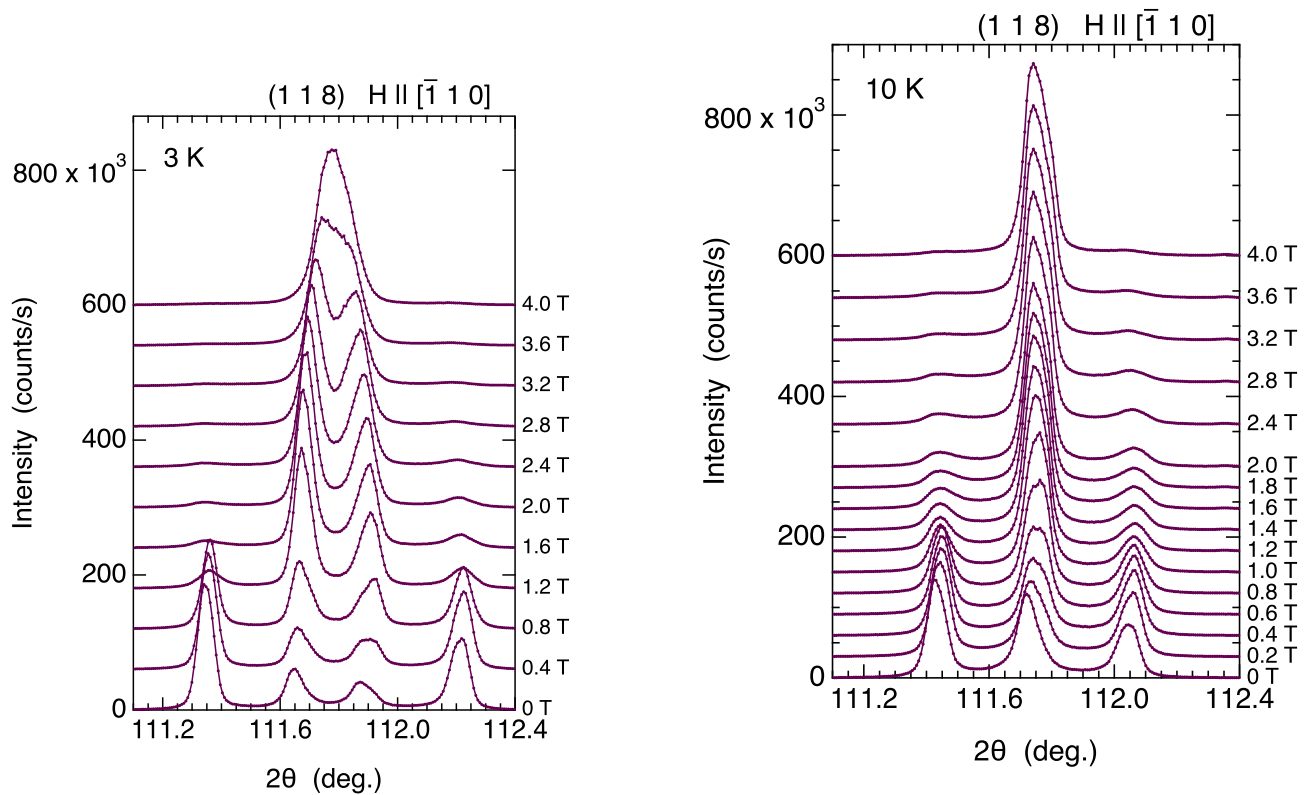


Fig. S6. Scattering angle (2θ) dependences of the intensity of the (1 1 8) reflection at 3 K in magnetic fields applied along $[\bar{1} 1 0]$. The intensities of the outer peaks abruptly decrease at 1 T and transfer to the inner peaks. The width of the peak split between the inner peaks gradually decrease and merge back into the central peak above 4 T. The intensities of the outer peaks weakly remain up to 4 T, which seems to remain even at 6 T very weakly (see the logarithmic plot in Fig. S4).

Fig. S7. Scattering angle (2θ) dependences of the intensity of the (1 1 8) reflection at 10 K in magnetic fields applied along $[\bar{1} 1 0]$. The intensities of the outer peaks exhibit a steep decrease at around 1 T and a gradual decrease up to 4 T. The decreased intensity is transferred to the central peak. The intensities of the outer peaks weakly remain up to 4 T, which seems to remain even at 6 T very weakly (see the logarithmic plot in Fig. S4). The field dependence of L in (H, K, L) for (1 1 8) shown in Fig. 7 in the main text are obtained from these data of Figs. S6 and S7.

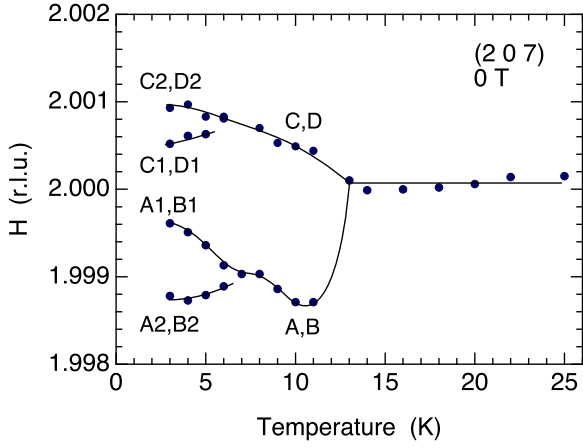


Fig. S8. Temperature dependence of the peak position of the (2 0 7) reflection, H in (H, K, L) , expressed in the reciprocal lattice unit of the tetragonal lattice. The labels represent the domain assignments shown in Fig. 8 in the main text. The asymmetric and complex behavior of the peak position may be ascribed to the subtle change in the sample orientation due to the structural deformation. We took into account only the magnitude of the peak split to estimate the parameters of triclinic distortion.

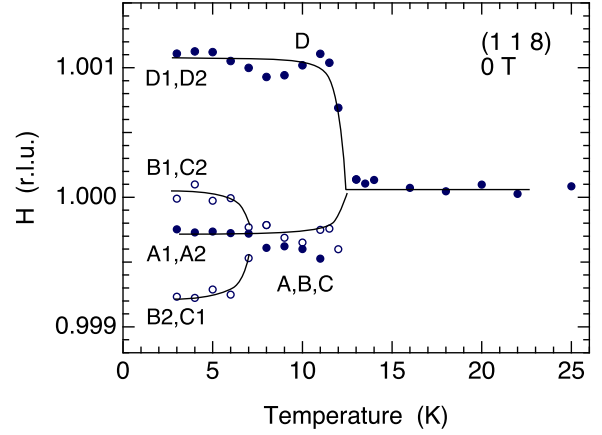


Fig. S9. Temperature dependence of the peak position of the (1 1 8) reflection, H in (H, K, L) , expressed in the reciprocal lattice unit of the tetragonal lattice. The labels represent the domain assignments shown in Fig. 8 in the main text. The asymmetric behavior of the peak position may be ascribed to the subtle change in the sample orientation due to the structural deformation.

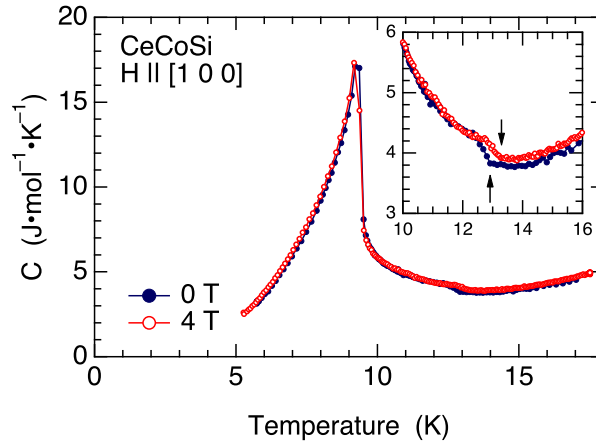


Fig. S10. Temperature dependence of the specific heat of the sample used in the X-ray diffraction in this study. The arrows in the inset indicate the anomaly at T_0 .

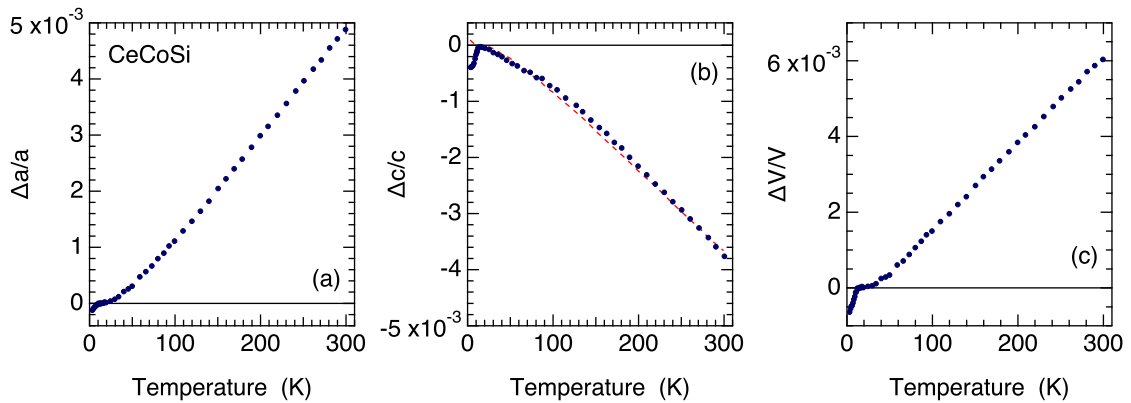


Fig. S11. Temperature dependences of the relative change in the lattice parameters (a) $\Delta a/a$ and (b) $\Delta c/c$. $a = 4.057 \text{ \AA}$ and $c = 6.987 \text{ \AA}$ at room temperature [H. Tanida *et al.*, J. Phys. Soc. Jpn. **88**, 054716 (2019)]. The lattice parameters were measured by using a laboratory based X-ray diffractometer with a Cu target. The $\Delta a/a$ and $\Delta c/c$ data were deduced from (4 0 0) and (0 0 8) reflections, respectively. The dashed line in (b) represents $-0.75(\Delta a/a)$. No splitting was observed in the (4 0 0) reflection because of the large crystal mosaicity of the side edge of the sample used in the measurement: plate-shaped with an as-grown c -plane surface, $1.5 \times 2.0 \text{ mm}^2$ in area and 0.3 mm in thickness. (c) Temperature dependence of the relative change in volume of the tetragonal unit cell.

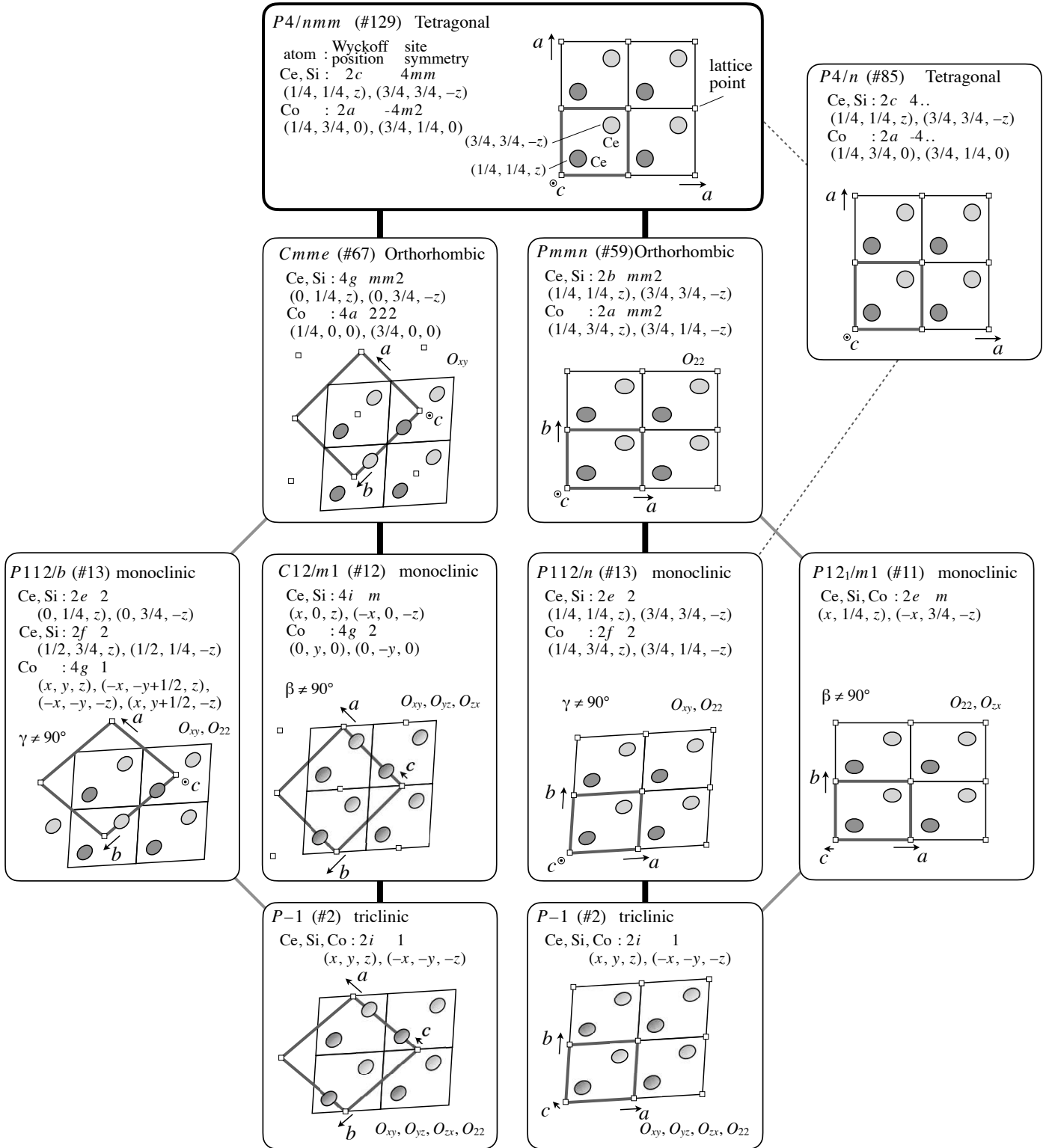


Fig. S12. Group-subgroup relations of CeCoSi from $P4/nmm$ (# 129) to $P\bar{1}$ (# 2) [International Tables for Crystallography, ed. T. Hahn (Springer, Heidelberg, 2005) Vol. A]. The thick black lines represent the likely processes we discussed in the main text. Ellipsoids schematically represent the quadrupole moments of Ce. Thick gray parallelograms represent the unit cell. Note that $Cmme$ (# 67) and $C12/m1$ (# 12) are C-centered. For $H \parallel [010]$, we proposed a possibility of the symmetry reduction from $Pmmn$ (# 59) at $T > T_0$, to $P112/n$ (# 13) at $T_{s1} < T < T_0$, and to $P\bar{1}$ (# 2) at $T < T_{s1}$. For $H \parallel [\bar{1}10]$, we proposed that it starts from $Cmme$ (# 67) at $T > T_0$ and is immediately reduced to $P\bar{1}$ (# 2) at $T < T_0$. The gray lines are the ones we consider unlikely. $P4/n$ (# 85), connected by the gray dashed lines, is not likely because the mirror symmetry is lost, which is not the case here. $P121/m1$ (# 11) for $H \parallel [010]$ and $P112/b$ (# 13) for $H \parallel [\bar{1}10]$ are unlikely because the experiment shows that the c -axis tilts toward the $[110]$ direction.